Eur. Phys. J. B **19**, 385–391 (2001)

THE EUROPEAN PHYSICAL JOURNAL B

EDP Sciences

Triplet-triplet interaction in a nearly one dimensional molecular crystal: Application to 1,4-dibromonaphtalene

A. Benfredj[1], D. Gamra[1], S. Romdhane[1], T. Barhoumi[1], C. Guthmann[2], J.L. Monge[2], and H. Bouchriha[1,2,a]

[1] Laboratoire de Physique de la Matière Condensée, Faculté des Sciences de Tunis, 1060 Tunis, Tunisia
[2] Groupe de Physique des Solides, Universités Paris 6 et Paris 7, Tour 23, 2 Place Jussieu, 75251 Paris Cedex 05, France

Received 12 March 1999 and Received in final form 27 April 2000

Abstract. The effect of a magnetic field (6 kG) on the delayed fluorescence in a 1,4-Dibromonaphtalene at 300 K and 20 K is analysed using a new approach of calculation of the triplet-triplet annihilation rate constant. The agreement of the best fit between experiment and theory allows reaching at 300 K and 20 K respectively the lifetimes and the interaction constant of the triplets pairs.

PACS. 32.30.Dx Magnetic resonance spectra – 32.50.+d Fluorescence, phosphorescence (including quenching) – 71.35.-y Excitons and related phenomena

1 Introduction

Many studies have been performed on triplet excitons dynamics in aromatic hydrocarbon crystals; it has been established that triplet excitons can cover macroscopic distances at room temperatures [1–4], consequently there is a high probability of formation of triplet excitons pairs that can lead to higher excited levels in the crystal.

In most cases [2], these levels are singlet excitons, which have a radiative decay providing a delayed fluorescence by the lifetime of the triplet excitons.

The modulation of this fluorescence by a magnetic field is a powerful tool in order to study the motion of free triplet excitons and the probabilities of formation and dissociation of triplet pairs. Theoretical models were established and have given a detailed view of triplet interaction mechanism in several molecular crystals [2,3].

However, these studies were essentially performed in two and three dimension excitons motion systems. The case of one, or nearly one-dimensional systems, is not well developed [5].

Recently, we have developed a modification of the so-called "Suna method" which was successfully applied to magnetic field effect in some 2D and 3D systems [6].

In this paper we extend this approach [6] to the case of a nearly one dimensional exciton motion system, for the interpretation of experimental results obtained on the modulation of delayed fluorescence at room temperature and at 20 K in the 1,4-DBN.

[a] e-mail: habib.bouchriha@fst.rnu.tn

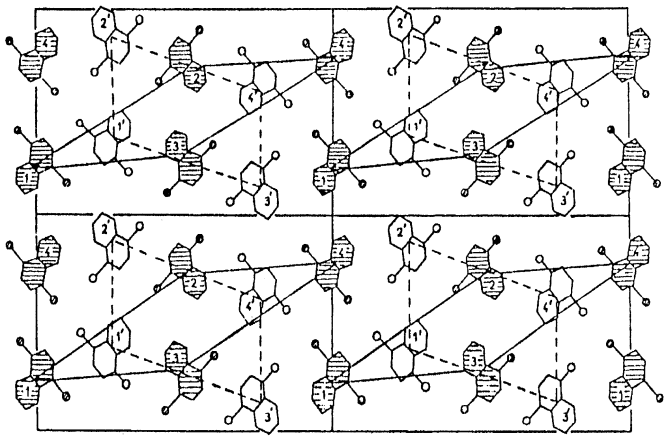

Fig. 1. Projection of DBN crystal structure parallel to the c-axis [2,4].

2 Experimental results

1,4-DBN is a monoclinic P_{2_1} crystal made of stacks of molecules piled up along the c-axis (Fig. 1) [7].

Direct measurements of the triplet excitons diffusion tensor at 300 K by optical spectroscopy at 4 K [8,9], and by triplet ESR measurements from 2 to 300 K [8,9], showed that the motion of triplet excitons is very nearly restricted to linear chains of molecules stacked along the c-axis crystal.

Crystalline samples of 1 to 3 mm thick are obtained by cutting and polishing sections from crystal ingots grown from the melt of highly purified 1,4-DBN. The faces are parallel to (ab), (ac') or (bc') crystal planes.

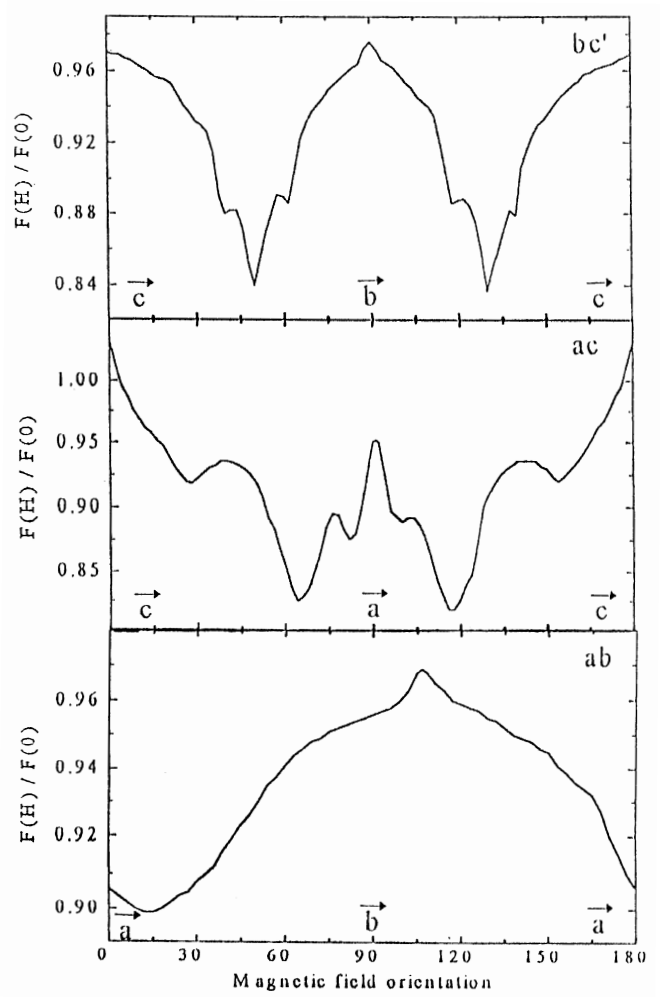

Fig. 2. Anisotropy of high static magnetic field (6000 G) effect on delayed fluorescence in bc', ac' and ab planes of DBN crystal at 300 K.

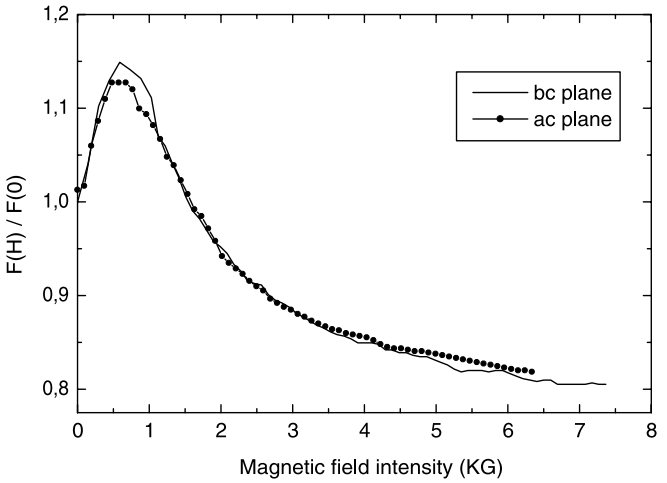

Fig. 3. Variation of delayed fluorescence intensity with magnetic field strength for an applied field in the directions where the effect is maximal in bc' and ac' plane, at 300 K.

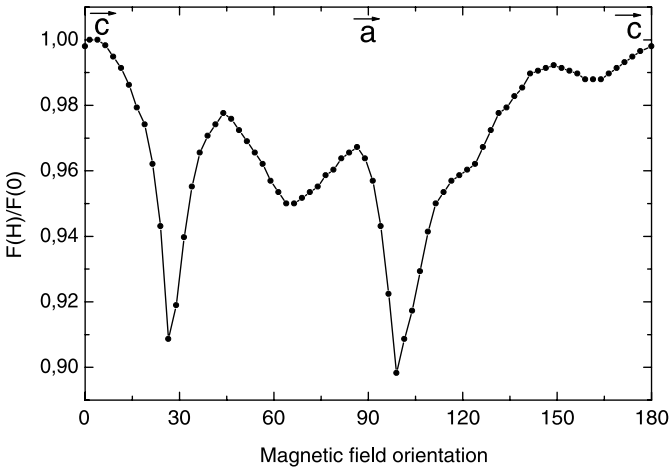

Fig. 4. Anisotropy of high static magnetic field (6000 G) effect on delayed fluorescence in the ac' plane of DBN crystal at 20 K.

The experimental set up is well described in [10]. The sample is placed between the pole pieces of an electromagnet and the magnetic field is rotated in a horizontal plane through 360°. The sample is excited directly in the lowest triplet state by the 4880 Å line of an argon laser through a corning CS3-70 filter. The delayed fluorescence is sent to a photomultiplier by a light guide and through two corning CS7-60 filters. All experiments are performed at low triplet density. The signal is sent to a lock-in analyser and accumulated into a microcomputer.

For low temperature experiments, the sample is introduced a coventional optical cryostat capable of reaching 20 K.

Figure 2 shows the anisotropy of a high magnetic (6 kG) field effect on the delayed fluorescence in the (ab), (ac') and (bc') crystallographic planes at room temperature. The effect exhibits maxima and minima for particular orientations of the magnetic field. The maxima, so-called "resonances", corresponds to a degeneracy of triplet pair state energy levels and their positions allow [5] the identification of the types of triplet-triplet annihilation. The sharp minima, corresponding to an enhancement of fluorescence are contrary to the current theories and our aim is to explain them and to fit the anisotropy effects in taking into consideration all types of annihilation.

In Figure 3 we exhibit the variation of the delayed fluorescence intensity with the magnetic field strength for an applied field in the directions where the effect is maximal in bc' and ac' planes.

The anisotropy of a high magnetic (6 kG) field effect on the delayed fluorescence in the ac' plane at 20 K is shown in Figure 4.

3 Theoretical model

The theoretical approach is developed in reference [6], and applied with success on two and three dimensional excitonic diffusion systems.

For a uniform density of excitons and in monomolecular regime, the mutual annihilation rate constant of triplet

exitons is considered as being [2]:

$$\gamma = \frac{1}{\eta^2}\int_0^\infty \Lambda(r)F(r)\mathrm{d}v, \tag{1}$$

where n is the uniform exciton density; $\Lambda(r)$ is the spin independent annihilation probability of two r distant excitons and $F(r)$ is the two stationary particles distribution function.

To take coherent and stochastic processes into account we use the density operator for triplet's pair $\rho(r)$ instead of $F(r)$.

$\rho(r)$ is the stationary value of $\rho(r,t)$ and is given by:

$$\begin{aligned}\frac{\partial\rho(r,t)}{\partial t} &= 0\\ &= \underbrace{-\frac{\mathrm{i}}{\hbar}[H_0,\rho(r,t)]}_{\text{Coherence}} - \underbrace{2\beta\rho(r,t)}_{\text{Decay}} - \underbrace{\lambda(r)[\tilde{\Lambda},\rho(r,t)]^+}_{\text{Annihilation}}\\ &\quad + \underbrace{2D\nabla^2\rho(r,t)}_{\text{Diffusion}} - \underbrace{R\rho(r,t)}_{\text{Relaxation}} + \underbrace{Q}_{\text{Creation}}.\end{aligned} \tag{2}$$

$[\ ,\ ]^+$; anticommutator divided by two and R is the relaxation supermatrix.

Respectively, the right side terms of this equation stand for coherence, monomolecular decay, interaction, diffusion, relaxation and creation of the triplet pairs.

H is the sum of the free triplet Hamiltonians without interaction

- β is a pseudo molecular decay constant and is proportional to the probability of an exciton to escape from the 1D system with no future interaction.
- $\lambda(r)$ is given three values (∞, λ, 0) around each exciton. There are three zones:
  $0 < r < r_\mathrm{a}$: impossibility to find two excitons on the same molecule ($\lambda(r) = \infty$).
  $r_\mathrm{a} < r < r_1$: diffusion with interaction ($\lambda(r) = \lambda$).
  $r_1 < r$: diffusion with no interaction ($\lambda(r) = 0$).
- $\Lambda = sP_s + tP_t + qP_q$, P's being the projection operators of S, T and Q states of the pairs; s, t and q the relative importance of the three annihilation ways ($s + t + q = 1$).
- D is the 1D diffusion coefficient.
- ∇^2 is the Laplacian for 1D motion.
- R is the relaxation super matrix and computed according to the hopping model [6].
- Q is the source term with nine equi-populated levels ($Q \propto \frac{1}{9}I$, I is the unit matrix in Hilbert space).

The computation was made in dimensionless units with respect to 2β.

The matrices were written as column vector and supermatrices as matrices.

The superoperators are:

$$\begin{aligned}A &= -\frac{2\pi}{2\beta}\mathrm{i}\left[H\otimes I - I\otimes H^T\right] + I\otimes I\\ B &= \left[\tilde{\Lambda}\otimes I + I\otimes\tilde{\Lambda}^T\right]/2.\end{aligned} \tag{3}$$

Table 1. Molecules involved in the three annihilation types.

Type of annihilation	Molecules involved
intrastack	1-1 ; 2-2 ; 3-3 ; 4-4 1'-1' ; 2'-2' ; 3'-3' ; 4'-4'
interstack intrasite	1-2 ; 1-3 ;1-4 ; 2-3 ; 2-4 ; 3-4 1'-2' ; 1'-3' ;1'-4' ; 2'-3' ; 2'-4' ; 3'-4'
interstack intersite	1-1' ; 1-2' ; 1-3' ; 1-4' 2-1' ; 2-2' ; 2-3' ; 2-4' 3-1' ; 3-2' ; 3-3' ;3-4' 4-1' ; 4-2' ; 4-3' ;4-4'

Then the equation (2) becomes [6]:

$$\left[(A+R) + \tilde{\lambda}(r)B\right]X(r) - r_d^2\nabla^2 X(r) = X_0 \tag{4}$$

where:

- $r_d = \sqrt{\frac{2D}{2\beta}}$ and $\tilde{\lambda}(r) = \frac{\lambda(r)}{2\beta}$
- $X(r)$ is the vector column built with pair density matrix $\rho_{ij}(r)$ (Eq. (18) of Ref. [6]).

The B, A and R matrices are given by equations (19, 20) and (A.17) of reference [6].

To calculate the fluorescence quantum yield R_s we solve equation (4) for different values of $\lambda(r)$, taking the continuity of $\rho(r)$ *via* $X(r)$, and its derivative at $r = r_\mathrm{a}$ and $r = r_1$ into account.

R_s is given by:

$$R_s = 2\beta\Gamma^T\int_0^\infty \lambda(r)BX(r)\mathrm{d}v = 2\beta\Gamma^T[X_1 + X_2] \tag{5}$$

where Γ, X_1 and X_2 are given by equations (26, 28, 29) of reference [6].

4 Application to 1,4-DBN

The DBN crystal could be considered as made of eight independent one dimensional crystals, corresponding to the eight differently oriented chains (Fig. 1); the delayed fluorescence emitted by the sample is then simply taken as the sum of the eight different types of chain, each independently modulated by the magnetic field. Because of the symmetry relations in the unit cell, the number of independent possible resonances is smaller than eight: chains related by inversion give identical results, hence the maximum number of high field resonances corresponding to inchain annihilations is four pairs.

Table 1 shows the different types of triplet interactions, which could be classified in three types: intrastack (i-i and i'-i'), interstack intrasite (i-j or i'-j') and interstack intersite (i-j').

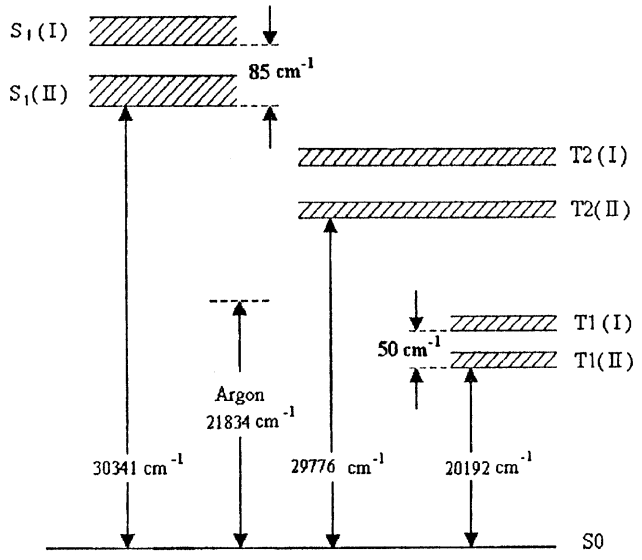

Fig. 5. The lowest energy levels of DBN crystal [4].

The magnetic field effect is then the sum of the modulation of the different types of interactions. These interactions do not occur with the same probability and we can write:

$$\frac{F(H)}{F(0)} = C_{i\text{-}i}\left(\frac{F(H)}{F(0)}\right)_{i\text{-}i} + C_{i'\text{-}i'}\left(\frac{F(H)}{F(0)}\right)_{i'\text{-}i'} + C_{i\text{-}j}\left(\frac{F(H)}{F(0)}\right)_{i\text{-}j} + C_{i\text{-}i'}\left(\frac{F(H)}{F(0)}\right)_{i\text{-}i'}. \quad (6)$$

At low temperatures and due to the 50 cm^{-1} splitting (Fig. 5), the four chains of site II are depopulated and the corresponding interaction should disappear. We can then have only two types of annihilation: intrachain and interchain intrasite.

5 Analysis of high field anisotropies

The approximate fitting of the anisotropy of the high magnetic field effect rotated in ab, ac' and bc' planes is shown in Figures 6–8.

To analyse this anisotropy we calculated the triplet pair states energies using the molecular ZF tensors for intrachain interactions and by taking average of the single-chain ZF tensors for interchain interactions. Table 2 gives ZF [11] parameters of the different types of interactions.

We also assumed that the diffusion coefficient is the same along the eight chains with the value: $D_{cc} = (3.5 \pm 0.8) \times 10^{-4}$ $\mathrm{cm}^2\,\mathrm{s}^{-1}$ [12]. We used for the action radius value the cell parameter along the c-axis ($r_\mathrm{a} = 4.09$ Å) and an intrachain interaction and neighbouring chains distance ($r_\mathrm{a} = 7$ Å and $r_\mathrm{a} = 10$ Å) for interchain interaction i-i' and i-j. For the interaction radius r_1 we take a value of $3r_\mathrm{a}$ for the four interaction types.

In Table 3 we give the different weights attributed to these interactions, and that shows the relative importance of these interactions on the resulting effect.

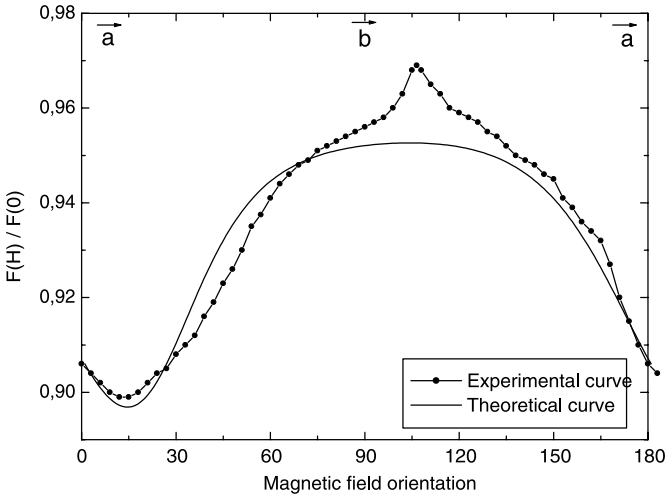

Fig. 6. The best fit of magnetic field anisotropy effect on delayed fluorescence in the ab plane of DBN crystal at 300 K.

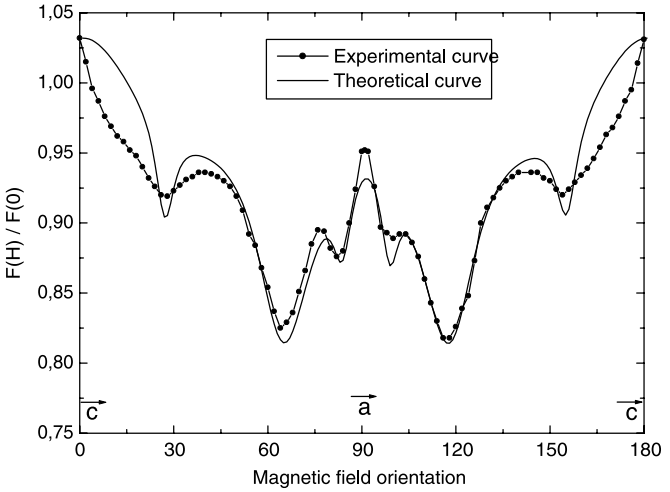

Fig. 7. The best fit of magnetic field anisotropy effect on delayed fluorescence in the ac' plane of DBN crystal at 300 K.

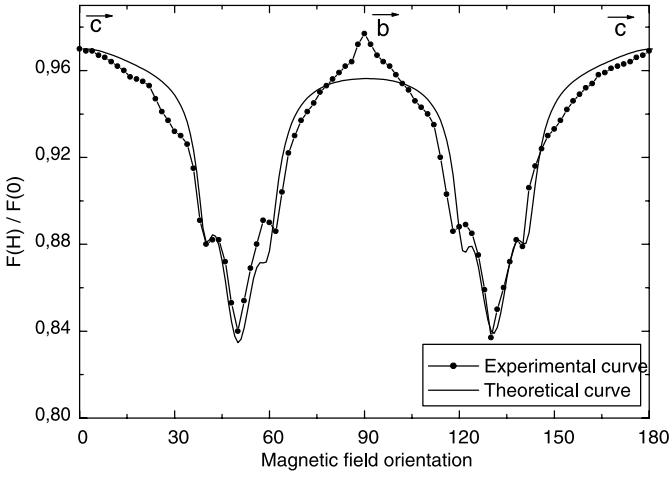

Fig. 8. The best fit of magnetic field anisotropy effect on delayed fluorescence in the bc' plane of DBN crystal at 300 K.

Table 2. Triplet exciton ZFS parameters.

INTERACTIONS	D (cm^{-1})	E (cm^{-1})	D* (cm^{-1})	E* (cm^{-1})	Fine structure tensor	Ref.
intrastack i-i	0.0968	0.0000	.....	.....	$\begin{pmatrix} & a & b & c' \\ x & -0.5414 & -0.7300 & +0.4171 \\ y & +0.6954 & -0.6676 & -0.2659 \\ z & +0.4726 & +0.1463 & +0.8690 \end{pmatrix}$	[11]
intrastack i'-i'	0.0968	0.0000	.....	.....	$\begin{pmatrix} & a & b & c' \\ x & +0.3594 & +0.8633 & +0.3543 \\ y & -0.8105 & +0.4770 & -0.3400 \\ z & -0.4625 & -0.1649 & +0.8711 \end{pmatrix}$	[11]
interstack intrasite i-j or i'-j'	0.0968	0.0000	-0.0453	-0.0474	$\begin{pmatrix} & a & b & c' \\ x & +0.8785 & +0.0000 & -0.4777 \\ y & +0.4777 & +0.0000 & +0.8785 \\ z & +0.0000 & +1.0000 & +0.0000 \end{pmatrix}$	[5]
interstack intersite i-j'	0.0968	0.0000	-0.0484	0.0249	$\begin{pmatrix} & a & b & c' \\ x & +0.0058 & -0.0107 & +0.9999 \\ y & +0.9488 & +0.3157 & -0.0021 \\ z & -0.3157 & +0.9487 & +0.0120 \end{pmatrix}$	[5]

Table 3. Different weights attributed to different annihilation types.

INTERACTIONS	Crystallographic planes	$\beta(10^8 s^{-1})$	$\lambda(10^{10} s^{-1})$	$\psi_\tau(10^9 s^{-1})$
Intrastack i-i	at 300 K ab	0.2	4	
	at 300 K bc'	0.2	4	
	at 300 K ac'	0.2	6	
	at 20 K ac'	20	0.4	
intrastack i'-i'	at 300 K ab	0.2	2	
	at 300 K bc'	0.6	2	
	at 300 K ac'	0.2	5	
	at 20 K ac'	27	1	
interstack intrasite i-j or i'-j'	at 300 K ab	1.5	6	0.5
	at 300 K bc'	2	4	0.5
	at 300 K ac'	2	4	0.5
	at 20 K ac'	15	0.4	0.5
interstack intersite i-j'	at 300 K ab	1	2.2	0.5
	at 300 K bc'	0.8	3	0.8
	at 300 K ac'	0.8	4	8
	at 20 K ac'	5	0.65	6

We can thus conclude that the weights attributed to the interchain intersite interaction (i-i') are decidedly superior to those assigned to the other interactions. This predominance can be explained by the greatest number of molecules involved in this type of interaction. In fact Table 1 gives a classification of the molecules involved in all types of interactions and permits to value comparatively the importance of each interaction.

The contribution of the interchain-intrasite interaction (i-j) is less important than the interchain-intersite interaction (i-j') but remains more important than those of intrachain interactions both, in ab and in bc' planes.

Table 4. Used parameters for the best fit to experimental curves.

Temperature	Crystallographic planes	$C_{i\text{-}i}$	$C_{i'\text{-}i'}$	$C_{i\text{-}j'}$	$C_{i\text{-}j}$
300 K	ab plane	0.1	0.1	0.6	0.2
	bc' plane	0.1	0.1	0.6	0.2
	ac' plane	0.075	0.15	0.7	0.075
20 K	ac' plane	0.025	0.75	0.2	0.025

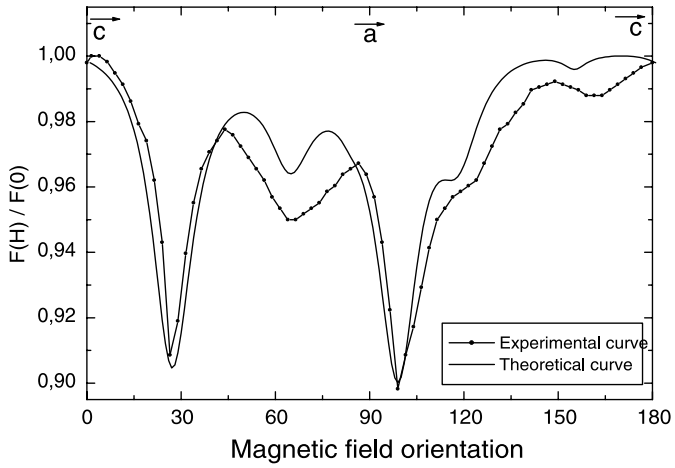

Fig. 9. The best fit of magnetic field anisotropy effect on delayed fluorescence in the ac' plane of DBN crystal at 20 K.

Table 1 gives also a plausible explanation to this noting since this type of interaction takes the second place concerning the number of molecules involved.

In the ac' plane, contrary to the other planes it is the intrachain interaction (i'-i') that takes the second place in the contribution to the global effect.

The best-fit parameters values are given in Table 4. The monomolecular decline constant, the inverse of which gives the lifetime of the exciton pair, increases when we pass from one dimensional motion (intrachain interactions) to a bidimensional motion (interchain interactions) for the three crystallographic planes.

The interaction constant λ, is of the same order of magnitude for all types of interactions and in the three crystallographic planes.

Finally, the hopping rate ψ_τ between non-equivalent molecules is of the same order of magnitude except for the interchainintersite interaction (i-i') in the ac' plane where it is six times larger.

Figure 9 shows the best fit of the anisotropy of the magnetic field effect on delayed fluorescence in ac' plane at 20 K. The different weights attributed to each interaction given in the Table 3 show that at low temperature only the intrasite interaction (i'-i') of the site II subsists. This is due to the fact that the sites present a splitting of 50 cm^{-1} for the lowest triplet excitation. At low temperature the site I is depopulated and its contribution is considerably reduced.

The best fit parameters, at 20 K in the ac' plane, are given in Table 4. We note that the decline constant β is larger when at 300 K, and this means that the lifetime of the exciton pairs is reduced for all interaction types.

We notice also a diminution of the interaction constant λ for all types of interaction and the higher value is attributed to (i'-i') interaction.

6 Discussion and summary

We have shown that the dynamics of excitons, in their intrachain motion, is statistically the same in both sites, which suggests that the stacks lengths are relatively short and that the average approximation is valid. This is also true for interchain interactions (intersites and intrasites).

We notice, however, that the intrachain-pairs lifetime is of the order of 5×10^{-8} s and is greater than the interchain-pairs lifetime which is of 5×10^{-9} s. This can be understood from the fact that interaction probability in one-dimensional motion is higher than those obtained for random motion in two or three-dimensional cases [13].

At low temperature, we notice that the lifetime decreases by an order of 10 to 100 times for interchain and intrachain interactions. This is probably due to the slowdown of the motion and also hence the decreasing of the diffusivity [14].

We observe, however, a clear decrease in the weights attributed to the interactions involving site I. This is due to the depopulation of this site, further to the 50 cm^{-1} splitting [9].

To complete this study we project to analyse the anisotropy of the effect for weak and medium fields and the variation of this effect with field intensity at low and at room temperature.

We also plan to perturb the Hamiltonian of the exciton pairs by a microwave field [15] in order to study the transitions between pairs spin states and to measure directly, by analysing the ODMR spectra, the triplet-triplet lifetime pairs involved in the different interaction types at room temperature.

References

1. S.M. Pimblott, A. Mozumder, Chem. Phys. Lett. **180**, 497 (1991); I.V. Zozulenko, A.I. Onipko, Sov. Phys. Solid State **30**, 1536 (1988); N.A. Efremov, S.G. Kulikov, R.I. Personov, Yu.V. Romanovskii, Sov. Phys. Solid State **31**, 407 (1989).
2. R.G. Kepler, J.C. Caris, P. Avakian, E. Abramson, Phys. Rev. **10**, 400 (1963); A. Suna, Phys. Rev. B **1**, 1716 (1970).
3. R.E Merrifield, Pure Appl. Chem. **27**, 481 (1971).
4. M. Pope, C.E. Swenberg, in *Electronic Processes in Organic Crystals* (Clarendon Press, Oxford, 1982).
5. H. Bouchriha, V. Ern, J.L. Fave, C. Guthmann, M. Schott, Chem. Phys. Lett. **53**, 288 (1978); A.N. Petrenko, Opt. Spect. **74**, 663 (1993).
6. A. Ben Fredj, S. Romdhane, J.L. Monge, H. Bouchriha, J. Phys. I France **7**, 349 (1997).
7. J. Trotter, Can. J. Chem. **39**, 1574 (1961).
8. R. Schmidberger, Dissertation, Universität Stuttgart, 1974.
9. G. Castro, R.M. Hochstrasser, J. Chem. Phys. **47**, 2241 (1967); R.M. Hochstrasser, J.D. Whiteman, J. Chem. Phys. **56**, 5945 (1972).
10. H. Bouchriha, M. Schott, J.L. Fave, J. Phys. France **36**, 399 (1975).
11. R. Schmidberger, H.C. Wolf, Chem. Phys. Lett. **16**, 402 (1972); **25**, 185 (1974).
12. V. Ern, J. Chem. Phys. **56**, 6259 (1972).
13. P. Avakian, A. Suna, Mat. Res. Bull. **6**, 891 (1971).
14. M. Mejatty, J.L. Monge, V. Ern, H. Bouchriha, Phys. Rev. B **36**, 2735 (1987).
15. M. Mejatty, J.L. Monge, V. Ern, H. Bouchriha, Phys. Rev. B **43**, 2558 (1991).